

Scattering and Multiple Scattering in NISP

P. A. Seeger*

Consultant, 239 Loma del Escolar, Los Alamos, NM 87544, U.S.A.

Abstract

It is very common to use Monte Carlo integration to estimate multiple scattering corrections in neutron experiments. The Neutron Instrument Simulation Package (NISP) includes various sample types and materials, many of which also account for multiple scattering. By combining the simulation of beam optics and multiple scattering, significant correlations are included. This report describes the implementation of multiple scattering in NISP, and shows the cross-section algorithms currently used. Source codes are available. An example of a full multiple scattering simulation is shown.

PACS: 28.20.Cz; 28.20.Gd; 21.60.Ka; 02.70.Uu

Keywords: Neutron scattering; Neutron instruments; Monte Carlo

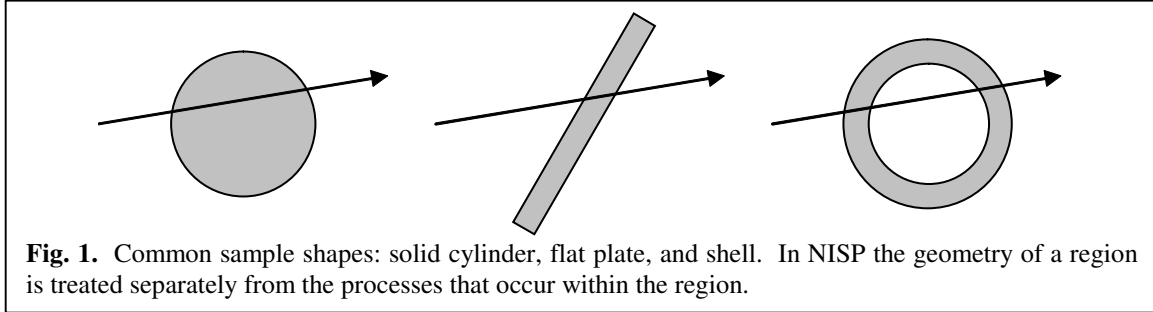
1. Neutron transport in dense materials

Common sample shapes for neutron scattering measurements include a cylinder or sphere, a flat rectangle or disk, and a cylindrical shell. These are illustrated in Fig. 1, with a typical neutron trajectory also shown. The Neutron Instrument Simulation Package (NISP) [1,2] treats the geometry separately from the contents of a region. When a neutron enters a region the distance D to escape is computed and passed to the `OPERATE` subroutine. (The source code for `OPERATE` and for all other procedures and files may be found through ref. [2].) In the case of a reentrant region such as the cylindrical shell, each segment of the trajectory is treated separately.

Various events can occur while a neutron passes through a material. It may cease to exist because of a nuclear reaction such as capture or (n,α) ; we refer to all such reactions as absorption and represent the sum of the cross sections as σ_a . (It should be noted that this formalism does not include *production* of neutrons through $(n,2n)$ or $(n,\text{fission})$ reactions.) The neutron may change direction without a significant change of energy; the sum of coherent and incoherent elastic scattering cross sections is called σ_s . Finally, the neutron may change both energy and direction through inelastic processes represented by cross section σ_i . All cross sections are multiplied by atomic density n (10^{24} atoms/cm³ or

* Corresponding author.

E-mail address: PASeeger@aol.com



atoms/barn-cm) to give “macroscopic cross sections,” $n\sigma$, with dimensions of cm^{-1} . The total macroscopic cross section is the sum of the three components:

$$n\sigma_t = n\sigma_a + n\sigma_s + n\sigma_i \quad (1)$$

There are two ways to apply probabilities when a random choice is to be made between possible processes. One is “analog” Monte Carlo, in which the outcome for each neutron is selected by comparing a uniform random deviate to the relative cross sections for the various processes. In NISP this method is used for simple materials that are used for structural members and filters. Since the principal use of such materials is absorption, we only use computer time to track a small fraction of non-absorbed histories. The other method, “weighted” Monte Carlo, is to split the incident neutron history into two or more fractional parts with appropriate statistical weights, and to track all possibilities. This is done in NISP for regions identified as samples. Thus we don’t lose histories due to absorption in the sample; *every* neutron that has managed to reach the sample through the incident collimation system is continued with its weight reduced to account for absorption.

Another case in which splitting may be used is polarization, which may occur either in simple materials or in samples. The projection of the incident neutron polarization on the magnetic field direction is used to find spin-up and spin-down probabilities, and the neutron history is either assigned one spin state or is split.

2. Transmission probability

We consider first the probability that the neutron passes through the material with no interaction. This is the transmission fraction,

$$T = \exp(-n\sigma_t D) \quad (2)$$

For simple materials a uniform random number R on $(0,1)$ is found, and if $T \geq R$ then the neutron escapes without modification. For samples the incident neutron is split into a transmitted and a scattered fraction, with the statistical weight of the transmitted neutron multiplied by T and the weight of the scattered neutron multiplied by $(1 - T)$. The neutron to be scattered is stored in a bank at the point (and time) where the trajectory entered the sample, and the tracking of the transmitted neutron is continued to its termination. In the case of the reentrant sample, the transmitted neutron after the first segment is split again where it reenters, and the scattered fraction for that segment is also stored in the bank.

When returning to treat the scattered neutron, we know that it has had some kind of interaction somewhere within a distance D along the trajectory. We have to determine what and where. The mean-free path is determined by the total cross section, so we find position by taking a sample from a truncated exponential distribution with parameter $(n\sigma_t)$ and maximum D , using function `PLEXP`. The neutron is then moved by the selected distance, and a nuclear collision occurs. The probability of absorption is the ratio $A = \sigma_a/\sigma_t$. For a simple material if A is greater than a uniform random number then the neutron is terminated, while for a neutron in a sample region the statistical weight is multiplied by $(1 - A)$ and the history is continued. That is, the neutron is split into an absorbed fraction (which is terminated) and a scattered fraction (which is tracked).

The essence of multiple scattering is as follows. A new direction is found, and a new value of the escape distance D is computed using the region and surface definitions which were passed to subroutine `OPERATE` for this purpose. If necessary (*e.g.* because of a change of energy) the cross sections are also recomputed. A new distance x is then taken from an exponential distribution with parameter $(n\sigma_t)$. If $x \geq D$, then the neutron escapes from the region with no further interactions (the transmitted fraction). If $x < D$, then the neutron is moved a distance x and another collision occurs, which may be either absorption or scatter. Every interaction in a sample reduces the statistical weight by a factor $(1 - A)$. This random walk is continued until the neutron is absorbed (simple materials only) or escapes through an external surface of the region. Some representative escaping neutrons are shown in Fig. 2, for elastic isotropic scatter in a solid cylinder. Although the scattering kernel is isotropic, the exponential penetration depth and multiple scattering generate a very anisotropic pattern. The pattern shown is for a single incident neutron trajectory; a complete Monte Carlo simulation integrates over all permitted incident paths.

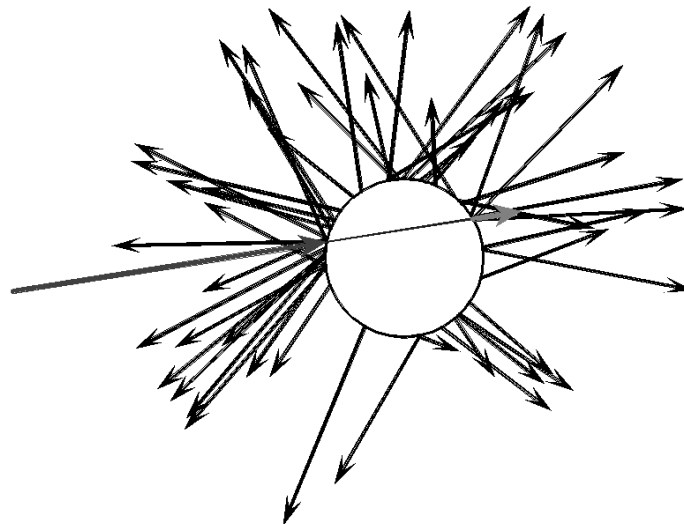


Fig. 2. Simulated multiple scattering in a cylindrical sample. The mean-free path is equal to the radius, and the probability of absorption at each collision is 20%. Scattering is isotropic in R^3 , shown projected on a horizontal plane. Vector length represents statistical weight, which is reduced at each interaction; the average of the 50 cases shown is 52.2% scattered and 32.4% absorbed, corresponding to an average of 2.16 collisions.

3. Cross-section algorithms

Several algorithms are available in NISP for estimating cross sections in various materials (region types 0–9 in the following list) or samples (region types 30–39). Some elements of other classes may also include scattering. The parameters for each region type are defined in file `MC_ELMNT.INC` [2], and the algorithms are found in subroutine `OPERATE` or in routines called from `OPERATE`. Many cross sections are proportional to $1/v$ or the neutron wavelength $\lambda = h/mv$, where $h/m = 0.0039560339 \text{ \AA}\cdot\text{m}/\mu\text{s}$ and v is the neutron velocity ($\text{m}/\mu\text{s}$). Not all types include multiple scattering.

It should be noted that most of the existing algorithms are simple and fast, designed to measure instrument resolution and to approximate backgrounds in a variety of configurations. For an indication of how to incorporate more detailed models for analysis of experimental data, see type 34. The stated parameters are those actually used in the algorithms; values requested by the interface (`MC_Web` or `NISP_Win`) may be different and are converted by the interface to the required numbers.

- 0 total absorber; no scatter, transmission, or surface optical reflection.
- 1 amorphous unpolarized material. Parameters are real and imaginary scattering-length density $nb = nb' + inb''$ ($10^{10}/\text{cm}^2$), high-energy macroscopic cross section (m^{-1}), and velocity-dependent macroscopic cross section at $v = 1 \text{ m}/\mu\text{s}$ (μs^{-1}). The absorption cross section is derived from the imaginary scattering length [3],

$$n\sigma_a = 2 \times 10^4 \lambda nb'' \quad (3)$$
 in units of m^{-1} . Scattering is elastic and isotropic, and multiple scattering is computed. Reflection or refraction may occur at the surface.
- 2 aluminum. Absorption only. Attenuation length from function `ATTEN_AL`, from Carpenter *et al.* [4].
- 5 beryllium. Absorption only. Attenuation length from function `ATTEN_BE`.
- 6 single-crystal filter. Absorption only. Attenuation length from function `ATTEN_X`, which uses the formalism of A.K.Freund [5].
- 7 nuclear resonances, including spin dependence for polarized neutrons. Examples are Cd, Sm, Au, and ^{240}Pu . Function `SINGLEEV` uses a generalized 1-channel R-matrix formalism [6]. Each cross section is a sum of resonances and non-resonant terms in isotope-spin channels.
- 13 crystal monochromator. Multiple scattering in mosaic crystals is treated (function `LMONOCRM`) by taking multiple fixed-length steps through the crystal, with reflection, transmission, absorption, and isotropic scattering computed at each step by a full solution of the Darwin equations [7].
- 30.0 small-angle scatter at constant Q . Momentum transfer Q ($/\text{\AA}$) is a given parameter.

30.2 small-angle scatter from hard spheres of constant radius. For each interaction a random value of QR is found by interpolation in tables of the cumulative Rayleigh scattering law [8] (function `PLQSPHR`) and divided by the specified radius R (\AA) to get Q ($1/\text{\AA}$). There is an upper limit of $Q_{\max} = 4\pi/\lambda$.

30.4 small-angle scatter proportional to $1/Q^2$. For each interaction, Q is selected by dividing parameter Q_{\min} ($1/\text{\AA}$) by a uniform random number on $(0,1)$. For all type 30 regions the scattering cross section is taken to be proportional to λ^2 and absorption is ignored. After Q is selected the scattering angle with respect to the incident velocity vector is found by

$$\sin(\theta/2) = Q\lambda/4\pi \quad (4)$$

Note that the exact angle is used, and not a small-angle approximation. Thus the allowed values of Q are not necessarily limited, but no scattering can occur if $\lambda > 4\pi/Q$. The azimuthal angle is random on $(0,2\pi)$, and subroutine `ELSCAT` is used to generate the new direction vector after each scatter.

32.0 isotropic scatter with fixed neutron energy gain, ΔE (meV); may be 0 for elastic scatter or < 0 for neutron energy loss.

32.2 isotropic scatter with multiple δ -function energy levels. The particular level to use is selected by comparing a random number to the normalized cumulative weights of the levels.

32.4 isotropic scatter with multiple energy levels and widths. As 32.2, with the selected level modified by a corresponding distribution (Lorentzian or Gaussian).

32.6 isotropic elastic scatter with absorption and multiple scatter. The scatter fraction $1-A$ is a parameter.

For all type 32 regions, the total cross section is proportional to $1/v$, or to λ . After accounting for transmission, the selected energy is added to the incident neutron energy. If the result is positive then scattering will occur. The direction after scatter is random in 4π . Multiple scattering is possible only for case 32.6, which was the type used to generate Fig. 2.

34.0 inelastic scatter using an $S(\alpha,\beta)$ file from MCNP [9]. Parameters α and β are dimensionless quantities representing Q^2 and ΔE [10]. The model includes inelastic and elastic cross sections and angular distributions, selected as a function of initial energy by subroutine `KERNEL` from a Type 1 thermal data table from MCNP. There is no absorption in this model.

34.n user defined inelastic scattering (n even). Other scattering models can be incorporated by linking to a different version of subroutine `KERNEL`. The parameters in the subroutine call are (passed by reference):

`FNAME` = complete path to file containing parameters and tables (input)
`E` = energy of the incident neutron in meV (input)
`EPRIME` = energy of the scattered neutron in meV (output)
`COS2TH` = cosine of the scattering angle, 2θ (output)
`MFP` = total mean-free path in mm (output)
`SCATFRAC` = scattering fraction, $1 - A$ or σ_s/σ_t (output)

ISEED = seed for the random number generator (input/output)

There are many recent publications of Monte Carlo scattering algorithms which it would appear could be implemented within this framework instead of stand-alone codes [11-15]. In particular, ref. [15] has a useful discussion of various statistical approaches that may be used.

For all type 34 regions, the azimuthal angle about the initial vector is uniform on $(0, 2\pi)$. Multiple inelastic scattering continues until the neutron escapes.

- 36.0 scatter from an isotropic polycrystalline powder. Subroutine `POWDER` uses the algorithm of Wildgruber & Passell [16]. Absorption and incoherent scatter are linear functions of λ , the same for all collisions of a given neutron. There is a table of decreasing Bragg d -spacings and a table of the corresponding cumulative cross sections (at $\lambda = 1 \text{ \AA}$), generated by Lazy-Pulverix [17]. The number N of possible Bragg reflections is a function of λ , and the coherent cross section varies as λ^2 below each Bragg edge. Thus for a given λ ,

$$n\sigma_{\text{coh}} = n\sigma(\lambda_N) \lambda^2 \quad (5)$$

$$n\sigma_s = n\sigma_{\text{incoh}} + n\sigma_{\text{coh}} \quad (6)$$

For each interaction, a Bragg d -spacing is selected by comparing a random number to the table of cumulative cross sections, also allowing for incoherent scatter. The scattering (half-)angle θ is determined by the Bragg condition, or is isotropic:

$$\sin(\theta_{\text{coh}}) = \lambda/2d \quad (7)$$

$$\sin(\theta_{\text{incoh}}) = \sqrt{\text{(random number on } (0,1))} \quad (8)$$

For justification of eq.(8) see notes in `POWDER`. The selected angle and the cross sections are returned to `OPERATE` which performs the full multiple-scattering treatment. The azimuthal angle for each scatter is uniform on $(0, 2\pi)$ (`ELSCAT`).

4. Limiting the solid angle of scattering samples

In many scattering instruments the solid angle accepted by an analyzer or detector following the sample is a small fraction of 4π . To improve the efficiency of the simulation, it is possible for some samples to limit the azimuthal angle of the scattering event. This is often indicated by adding 0.1 to the sample type and providing parameters ϕ_{min} and ϕ_{max} . Such sample types are 30.1, 30.3, 30.5, 34.(n+1), and 36.1. The azimuthal angle with respect to the incident neutron velocity vector in these cases is uniform on $(\phi_{\text{min}}, \phi_{\text{max}})$, and *multiple scattering is turned off*. Subroutine `ELSCAT2` is called in place of `ELSCAT`, and the statistical weight is reduced by the acceptance fraction $(\phi_{\text{max}} - \phi_{\text{min}})/2\pi$.

An even more aggressive limitation of solid angle is provided for the isotropic scattering types (32.1, 32.3, and 32.5). The three direction cosines of the outgoing neutron velocity are chosen to be uniform between given min and max values for each axis. The accepted fraction of the sphere is computed in the interface and is given as a parameter.

These methods can not be used when multiple scattering is included, because we can't limit the angle of any single scattering event. Nor can we force the final event to go in the direction we want, because of the anisotropy (*cf.* Fig. 2). What we can do is to track multiple instances of the same incident neutron in hopes that one (and preferably only one) will be in the proper direction. When the scattered-fraction neutron is stored in the bank, it may be read back out a number of times with the statistical weight for each instance divided by the number of instances. The number is set by the run-time parameter `NSPLIT` in the Monte Carlo main program `MC_RUN`. To choose an appropriate splitting number, consider a binomial distribution with $p =$ acceptance fraction and $n =$ number of samples. Then if $P(m)$ is the probability that m neutrons are accepted,

$$P(m) = p^m (1 - p)^{(n - m)} n!/[m! (n - m)!] \quad (9)$$

To prevent correlations in the Monte Carlo results we must keep $P(>1)$ small, but we want $P(1)$ to be large. We can get a simple recipe for `NSPLIT` by considering the ratio

$$\alpha = P(2)/P(1) = [(n - 1)/2] p/(1 - p) \quad (10)$$

$$\text{NSPLIT} \approx n = 1 + 2\alpha(1 - p)/p \quad (11)$$

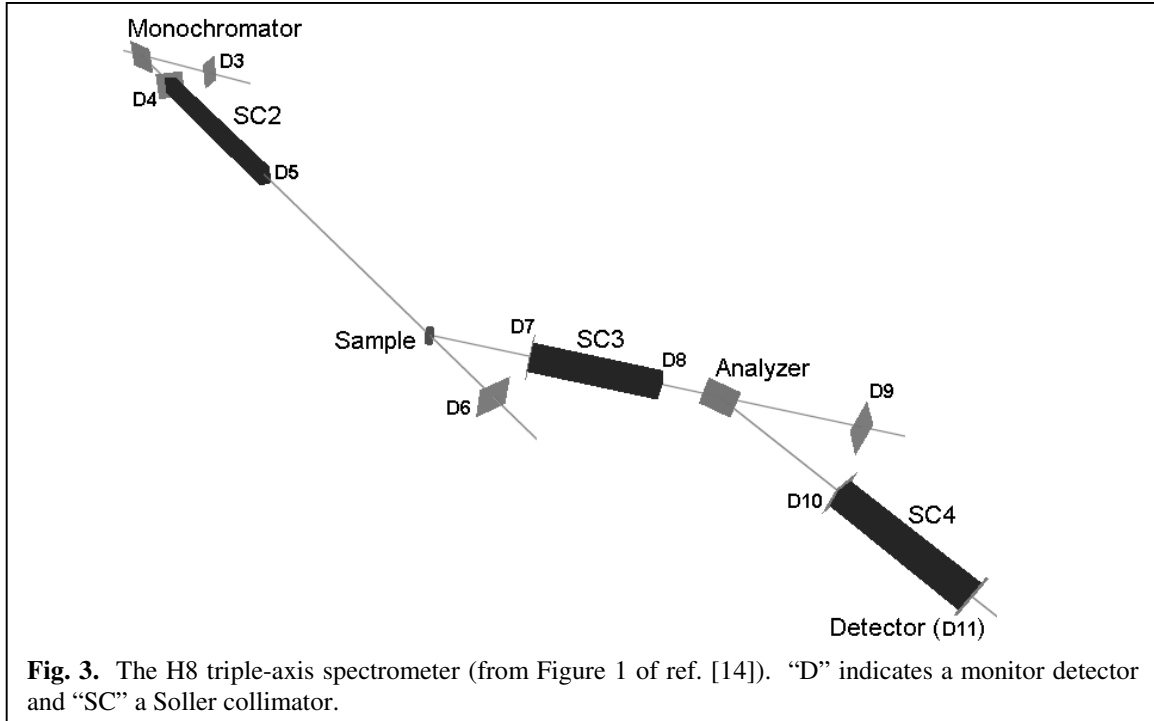
A reasonable value for α is 1/4; the effect of correlations is reduced because of the number of independent random events that occur in the sample itself. Then for instance if $p = 0.01$ we would use `NSPLIT` = 50, giving $P(0) = 0.60$, $P(1) = 0.31$, $P(>1) = 0.09$.

A reentrant sample such as the cylindrical shell in Fig. 1 is a special case. The splitting occurs each time the initial transmission-mode neutron enters or reenters the sample. Thus the value of `NSPLIT` should be half as great.

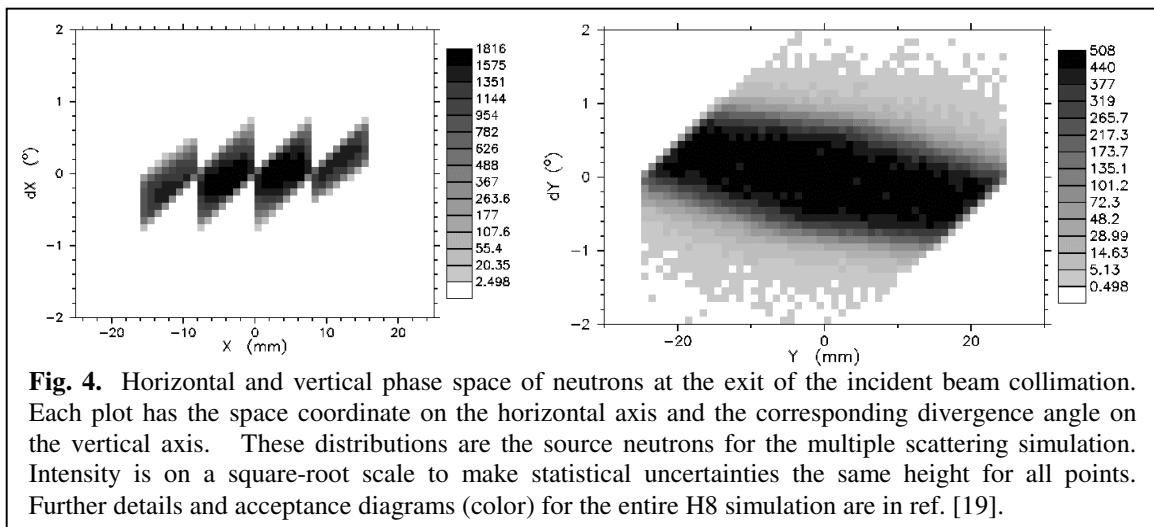
5. Example: vanadium sample in simulation of H8

In a recent publication [18], five Monte Carlo codes were used to simulate the same instrument, the H8 triple-axis spectrometer formerly installed at the HFBR, Brookhaven National Laboratory. The layout of the instrument following the monochromator is shown in Fig. 3. Figure 2 of ref. [18] shows that the agreement was pretty good before the sample, detector D5, and that the only two codes to report the sample transmission (detector D6) agree very well. However the agreement after scattering from the vanadium sample is not as good. We assumed this was because of differences in the treatment of absorption and multiple scattering in the sample. It will therefore be of interest to compare calculations with and without multiple scattering.

As a source we use a file of 497,048 neutron histories recorded at D5, the exit of Soller collimator SC2. The phase-space density diagrams are shown in Fig. 4. The horizontal diagram shows how the divergence is limited by the four slots of SC2, while the vertical diagram has a negative slope because of the bent monochromator crystal which focuses at the sample [19]. This demonstrates that the phase space density of the beam incident on the sample is far from uniform, which can impact the effect of multiple scattering. Only a full simulation of the instrument, as with NISP, can account for such correlations.



Since the sample is only 6.4 mm wide and 25.4 mm tall, the majority of these neutrons miss it. We have 77,594 histories on the sample, with a total statistical weight of 38,784 neutrons (the average weight is 0.5 due to a splitting at the monochromator). The entrance of the collimator (SC3) in the analyzer leg of the instrument has a solid angle of 0.042 ster. But neutrons can’t pass SC3 unless they are also aimed at its exit, called D8. The acceptance of D8 is determined by the horizontal collimation and the vertical height, giving solid angle 0.0012 ster and fraction of the sphere $p = 9.4 \times 10^{-5}$. From eq. (11) we can use the very large value $NSPLIT = 5300$. Such a large $NSPLIT$ will result in a long execution time.



The values for the V cross sections at $\lambda = 2.359 \text{ \AA}$ used in the simulation were

$$\begin{aligned} n\sigma_{\text{incoh}} &= n\sigma_s = 0.362 \text{ /cm} \\ n\sigma_a &= 0.476 \text{ /cm} \\ n\sigma_t &= 0.838 \text{ /cm} \end{aligned} \tag{12}$$

The corresponding parameters for an elastic isotropic sample with multiple scattering (region type 32.6) are

$$\begin{aligned} n\sigma_t &= \lambda (35.52 \text{ /m-}\text{\AA}) \\ 1 - A &= n\sigma_s/n\sigma_t = 0.432 \end{aligned}$$

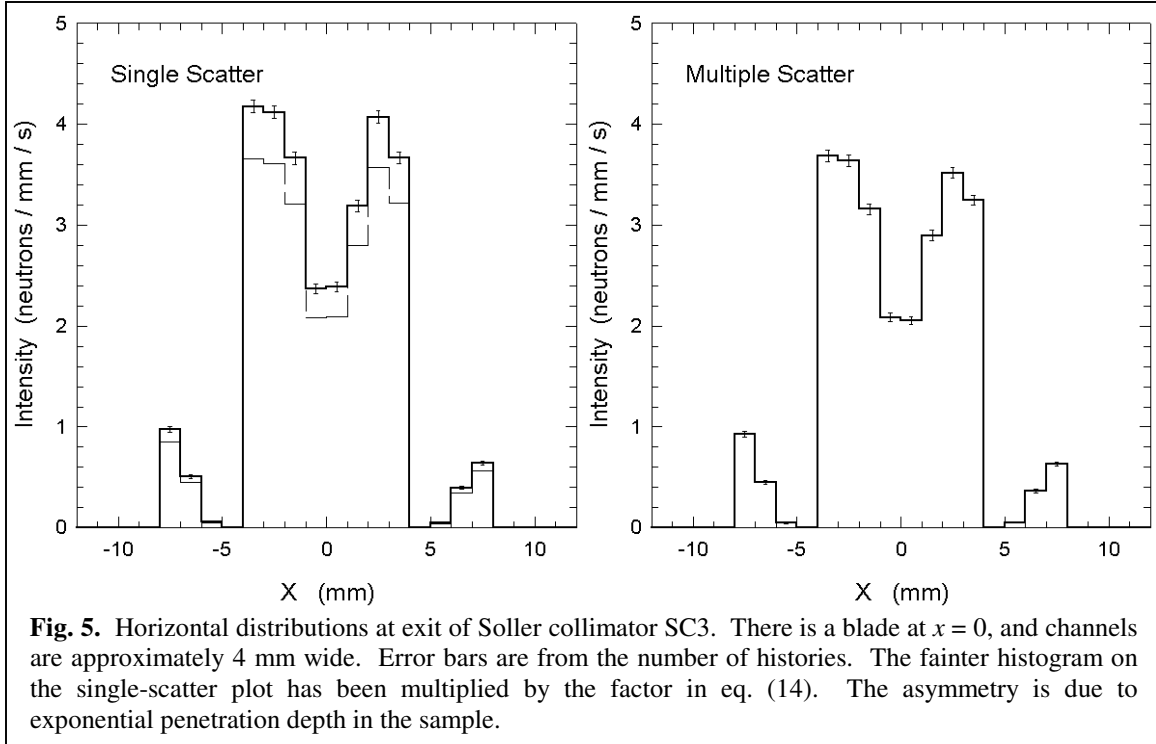
With these parameters the number of histories reaching D8 was 35,458, representing 0.4150 neutrons. The execution time (1.2-GHz Pentium-III) was 19 h 27 m, and the *rms* precision of the count rate in the final detector (D11 in Fig. 3) was 0.7%. We would more typically run for about 2 hours, which would give 2.3% precision in this case.

The execution time is *much* faster if multiple scattering is turned off and the solid angle of the scattering event is restricted. The allowed range in the horizontal direction is the nominal scattering angle \pm the sum of incident and exit collimation, or 39.68–42.67° (measured to the left from the beam axis). The vertical limits are determined by the heights of the sample and D8, giving $\pm 3.94^\circ$. We set the following direction-cosine limits:

$$\begin{aligned} \cos(\gamma_{\text{min}}) &= +0.7696 \text{ (39.68}^\circ \text{ from Z)} \\ \cos(\alpha_{\text{max}}) &= -0.6778 \text{ (132.67}^\circ \text{ from X)} \\ \cos(\beta_{\text{max}}) &= -0.0687 \text{ (93.94}^\circ \text{ from Y)} \\ \cos(\beta_{\text{min}}) &= +0.0687 \text{ (86.06}^\circ \text{ from Y)} \end{aligned} \tag{13}$$

The “rectangle” defined by these four latitude circles includes all of the required solid angle. (The other two possible limits, α_{min} and γ_{max} , are not needed.) The solid angle divided by 4π is 5.89×10^{-4} , as integrated numerically in either MC_Web or NISP_Win. We can also improve statistics by splitting; we chose `NSPLIT = 3` to get a similar number of histories as in the previous case. Then 32,556 histories reached D8 in an execution time of 2 m 27 s, or a factor of 440 faster per detected history than the multiple-scattering case. The number of neutrons (after correcting for the fraction absorbed in a single collision) was 0.4615, 11.2% higher than when multiple scattering was included.

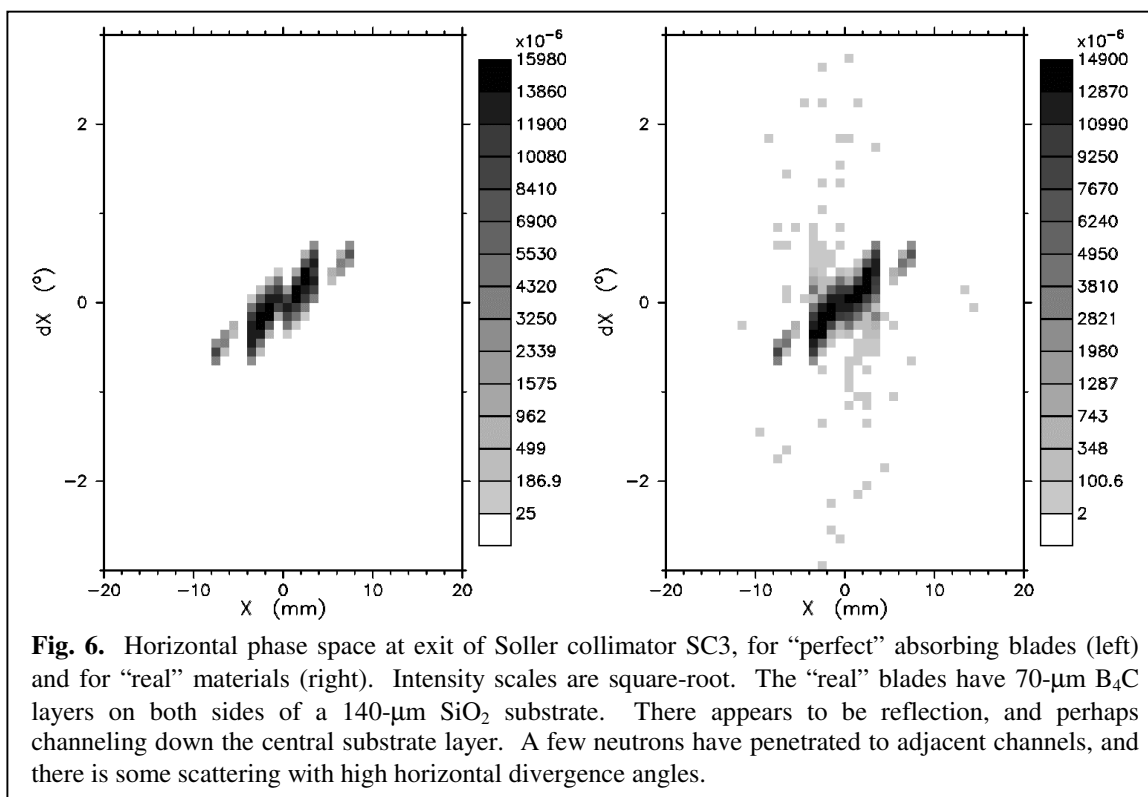
The horizontal distributions at the exit of SC3 for the two simulations are shown in Fig. 5. The error bars are Poisson statistics on the number of histories recorded, neglecting correlations. Within these statistics there is no difference in the shapes of the distributions beyond a constant factor. The asymmetry is significant and is the result of the exponential penetration depth in the sample; there are more neutrons on the left because there are more interactions near the front of the sample. The additional neutrons absorbed in the multiple-scatter case correspond to an average path length of 2.23 mm between the first scatter and escape. If we integrate the escape in a specific direction from uniformly distributed points in a circle of radius R , we get $\pi R/4$, which in this case is 2.51 mm. The first-order absorption correction factor would be



$$F = \exp(-n\sigma_a\pi R/4) = 0.887 \quad (14)$$

Applying this to the single-scatter result (Fig. 5) gives an integrated intensity 1.3% less than the multiple-scatter result.

We can also use this simulation to illustrate the effect of scattering in simple materials, by modifying the blades in Soller collimator SC3. In ref. [18] the blades were perfect absorbers, 0.280 mm thick. The simulation was rerun with blades consisting of 0.140 mm SiO_2 coated on each side with 0.070 mm of B_4C . The material in the interior was also changed from void to air. Because a very large number of histories was scattered out the top or bottom, the collimator was also surrounded by 1 cm of Fe; this did prevent neutrons from escaping, but many were scattered back into the collimator. The solid-angle limits in eq. (14) were increased by a factor of 3 in the horizontal plane so that a substantial number of histories would hit the blades. `NSPLIT` was also tripled to keep about the same statistics at D8. Execution time was not significantly increased. The integrated count rate was higher by 4%, and the shape of the distribution was not much different from Fig. 5. The difference can be seen most clearly in the horizontal phase-space distributions in Fig. 6. A few neutrons appear in slots at higher X , having penetrated a blade. The center is somewhat filled in, possibly due to channeling in the substrate; this would be improved by using a substrate with more attenuation. The largest component is reflection from the B_4C surface, shown by the mirror symmetry about the dX axis. The surfaces were left smooth to demonstrate this effect; making the surfaces rough greatly reduces reflection. Finally, there is a scattered component with quite large divergence angles. Many of these come from the surrounding shielding. Because of the large angles they are unlikely to be analyzed and reach the final detector. Neutrons that have backscattered from the analyzer crystal have been omitted from the figure.



6. Conclusion

Calculating multiple scattering using NISP automatically includes any correlations between the instrument design and the scattering sample. NISP is capable of a full multiple-scattering treatment, but it is costly in computer time; in the example presented the execution time factor was more than 400. For this example (6.4-mm diameter V, $\lambda = 2.359 \text{ \AA}$), a simple geometric factor applied to a single-scatter treatment provides a result close to the “true” value. The asymmetry due to penetration depth is more significant than multiple scattering in this sample. It will generally not be necessary to make any further corrections for multiple scattering when designing an instrument, but for data analysis the full treatment would be justified.

Another application of scattering in NISP is to identify and mitigate sources of backgrounds.

The author would gladly assist in implementation of additional scattering kernels.

References

- [1] P.A. Seeger, L.L. Daemen, T.G. Thelliez, and R.P. Hjelm, *Neutron News* **13** (2002) No. 4, p. 20; Proceedings of ICANS-XIV, June 14–19, 1998, ANL report ANL 98/33, vol. 1, p. 202.

- [2] <http://strider.lansce.lanl.gov/NISP/Welcome.html>. Source codes may also be downloaded from <ftp://strider.lansce.lanl.gov/pub/NISP/>. When using the codes in other environments, all authorship comments must be retained.
- [3] G.E. Bacon, *Neutron Diffraction* (Clarendon Press, Oxford, 1975), §5.6.
- [4] J.W. Carpenter *et al.*, IPNS Note 32, Jan. 16, 1986 (unpublished).
- [5] A.K. Freund, *Nucl. Inst. Methods* **213** (1983) 495.
- [6] J.E. Lynn and P.A. Seeger, *At. Data & Nucl. Data Tab.* **44** (1990) 191.
- [7] P.A. Seeger and L.L. Daemen, *Appl. Phys* **A74** (2002) S1458.
- [8] Lord Rayleigh, *Proc. Roy. Soc. (London)* **A90** (1914) 219; A. Guinier and G. Fournet, *Small-Angle Scattering of X-Rays* (Wiley, New York, 1955), p. 19.
- [9] J.F. Briesmeister (ed.), LANL report LA-12625-M (1993), p. 2-49 *ff*.
- [10] J.R.D. Copley, *Comput. Phys. Commun.* **7** (1974) 289; *J. Appl. Cryst.* **21** (1988) 639.
- [11] J. Dawidowski, F.J. Bermejo, and J.R. Granada, *Phys. Rev. B* **58** (1988) 706.
- [12] F. Carsughi, R.P. May, R. Plenteda, and J. Šaroun, *J. Appl. Cryst.* **33** (2000) 112.
- [13] J. Wuttke, *Phys. Rev. E* **62** (2000) 6531.
- [14] C.R. Borlando, F.J. Mompean, and R.L. Peng, *J. Appl. Cryst.* **34** (2001) 613.
- [15] J. Mayers, A.L. Fielding, and R. Senesi, *Nucl. Inst. and Meth. Phys. Res.* **A481** (2002) 454.
- [16] U. Wildgruber and L. Passell, July 14, 1995 (unpublished).
- [17] A.D. Murray and A.N. Fitch, ©1987; K. Yvon, W. Jeitschko, and E. Parthe, *J. Appl. Cryst.* **10** (1977) 73.
- [18] P.A. Seeger, L.L. Daemen, E. Farhi, W.-T. Lee, X.-L. Wang, L. Passell, J. Šaroun, and G. Zsigmond, *Neutron News* **13** (2002) No. 4, p. 24.
- [19] ftp://strider.lansce.lanl.gov/pub/NISP/document/H8_simJan29.doc